

Bloch oscillation of Weyl metal along synthetic dimensions

Ye Xiong(熊烨)

Citation: Chin. Phys. B . 2018, 27(12): 126701. **doi:** 10.1088/1674-1056/27/12/126701
Journal homepage: http://cpb.iphy.ac.cn; http://iopscience.iop.org/cpb

What follows is a list of articles you may be interested in

A combined system for generating a uniform magnetic field and its application in the investigation of Efimov physics

Rui Yao(姚睿), Zhen-Dong Sun(孙震东), Shu-Yu Zhou(周蜀渝), Ying Wang(王颖), Yu-Zhu Wang(王育竹)
Chin. Phys. B . 2018, 27(1): 016703. **doi:** 10.1088/1674-1056/27/1/016703

Two types of ground-state bright solitons in a coupled harmonically trapped pseudo-spin polarization Bose–Einstein condensate

T F Xu(徐天赋)
Chin. Phys. B . 2018, 27(1): 016702. **doi:** 10.1088/1674-1056/27/1/016702

Quench dynamics of ultracold atoms in one-dimensional optical lattices with artificial gauge fields

Xiaoming Cai(蔡小明)
Chin. Phys. B . 2017, 26(8): 086701. **doi:** 10.1088/1674-1056/26/8/086701

Landau damping in a dipolar Bose-Fermi mixture in the Bose-Einstein condensation (BEC) limit

S M Moniri, H Yavari, E Darsheshdar
Chin. Phys. B . 2016, 25(12): 126701. **doi:** 10.1088/1674-1056/25/12/126701

Spin excitation spectra of spin–orbit coupled bosons in an optical lattice

Li Ruo-Yan, He Liang, Sun Qing, Ji An-Chun, Tian Guang-Shan
Chin. Phys. B . 2015, 24(5): 056701. **doi:** 10.1088/1674-1056/24/5/056701

SPECIAL TOPIC — 60th Anniversary of Department of Physics of Nanjing Normal University

Bloch oscillation of Weyl metal along synthetic dimensions*

Ye Xiong(熊烨)†

Department of Physics and Institute of Theoretical Physics, Nanjing Normal University, Nanjing 210023, China

(Received 22 August 2018; revised manuscript received 12 November 2018; published online 25 November 2018)

Synthetic dimensions in time (Sambe space) can be utilized in a periodic time-dependent system. By subjecting the system into a time-periodic potential and measuring the physical quantities at distinct time in one period, one is able to simulate the models in higher dimension. To verify this approach, we show that the Bloch oscillation of wave packets along the magnetic field in a three-dimensional (3D) Weyl metal can be simulated on a two-dimensional (2D) insulator. Different from the chiral anomaly, this Bloch oscillation is anisotropic when the initial wave packet is not on the 0-th Landau level.

Keywords: synthetic dimensions, Weyl metal

PACS: 67.85.–d, 03.75.Lm, 74.20.Rp **DOI:** 10.1088/1674-1056/27/12/126701

1. Introduction

In many experiments, especially in those on the cold atoms, it is sometime hard or impossible to achieve the desired three-dimensional (3D) or higher-dimensional Hamiltonian in the real space.[1] To overcome this restriction, synthetic dimensions (SDs) are often proposed to play the role of the extra dimensions on a physical lower-dimensional system.[2–10] SD is usually realized by two methods. One is from scale parameters introduced to simulate the good quantum numbers, *e.g.*, the momenta k's in the SDs ($\hbar = 1$ is taken).[6–8,10] For instance, a one-dimensional (1D) Aubry–Andre model, $H = \sum_i [c^\dagger_{i+1} c_i + \text{h.c.} + 2t_y \cos(\alpha i + k_y) c^\dagger_i c_i]$ is equivalent to the Hamiltonian of a two-dimensional (2D) quantum Hall lattice when the scale parameter k_y is considered as the momentum along the synthetic direction y.[11–13] The other method is to engage suitable internal degrees of freedom. For instance, internal orbitals are proposed to act as the source of SD to simulate a four-dimensional (4D) model on a 3D physical system.[4,5,14,15] We are motivated by the other possibility of introducing the SDs.

In dealing with the time axis, the last successful story is the time crystals.[16–20] It extended the idea of the spontaneous breaking of the translational symmetry to the time axis. But if one want to treat the time as an SD, a principal obstacle is faced: The time and the space are playing different roles in the non-realistic Schrödinger equation. It is the space that actually provides the stage (Hilbert space) and the time is only used to describe how the wavefunction is dancing on it. It seems impossible to mix this picture by extending the stage to the time axis.

A more relevant topic to the question appears in the Floquet framework.[21–43] When the Hamiltonian is varying periodically with time,

$$H(t) = H(t+T). \tag{1}$$

Floquet method is used to study the quasi-static states

$$|\psi_n(t+T)\rangle = \mathrm{e}^{-\mathrm{i}E_n t}|\psi_n(t)\rangle,$$

where T is the period and $0 < E_n \leq \omega$ is the quasienergy. In calculating these E_n, Fourier transform is enrolled and the problem is mapped to a search of eigenvalues in a Floquet lattice with an inclined potential. Although the Floquet lattice enlarges the original lattice by an extra dimension, in which the number of photons attached to each site is playing the role of the new degrees of freedom, we are not considering it as the SD because the Floquet lattice is more likely a technical method to calculate the quasienergies. This opinion is supported by the fact that the Hilbert space of the quasi-static states $|\psi_n\rangle$ is not really enlarged finally.

In this paper, we use the metric in space to understand the framework of extended Hilbert space (Sambe space).[44,45] This explain why the detailed evolution within each period, which has been omitted in the Floquet framework, is crucial for the creation of the SD. The Hilbert space is enlarged by a method similar to that in the Floquet framework, but this virtual enlarged space is made synthetic only when a connection is established between the evolutions started at distinct times. To clarify these ideas, a redefinition of the inner product is flexible. We will define the inner production of two wavefunctions as $\langle\tilde{\psi}_a|\tilde{W}|\tilde{\psi}_b\rangle$, where $\tilde{W}$ is a metric. We will illustrate that at any instance time, the rank of the metric is much smaller than the dimension of the virtual Hilbert space. But as long as the metrics at every distinct times within one period are appended together, the total metric is fully ranked and

*Project supported by the National Natural Science Foundation of China (Grant No. 11774177).

†Corresponding author. E-mail: xiongye@njnu.edu.cn

© 2018 Chinese Physical Society and IOP Publishing Ltd

the SD is created. The modulated time, t mod T, will play the role of momentum in the SD. Interestingly, although there is only one axis in the time, the SDs generated from the time can be as many as needed. This makes the simulation of a higher-dimensional model on a physical lower-dimensional system be easily realized.

By applying these ideas, we show how to synthesize a 3D Hamiltonian on a 2D system. The 3D Hamiltonian is a Weyl lattice in parallel magnetic and electric fields. In such lattice, the Hamiltonian evolution of a wave packet can be symmetric or asymmetric in the direction of the fields, which can be traced back to the linear dispersion near the Weyl points. While such diffusion can be observed exactly on a 2D periodic time-dependent model subjecting to only magnetic field.

2. Synthetic dimension in time

We define a series of virtual time-dependent basis,

$$|n,i\rangle(t) = \mathrm{e}^{-\mathrm{i}n\omega t}|i\rangle, \tag{2}$$

where $\omega = 2\pi/T$ is the angular frequency and n takes all integer numbers. For the sake of clarity, we will truncate n by N in our expressions but the case with infinite n's can be easily restored. The virtual Hilbert space will be defined on the basis $\{|n,i\rangle\}$ and the direction along n is called the virtual direction (becoming the SD when the full rank metric is obtained). All operators and wavefunctions in the virtual Hilbert space will be expressed by tilde symbols.

For the basis $\{|n,i\rangle\}$, the inner product of the states gives $\langle n,i|m,j\rangle = \delta_{ij}\mathrm{e}^{-\mathrm{i}(m-n)\omega t}$. Equivalently, one can change the definition of the inner product to $\langle\tilde{\psi}_a|\tilde{W}|\tilde{\psi}_b\rangle$ with a metric $\tilde{W}_{ni,mj} = \delta_{ij}\mathrm{e}^{-\mathrm{i}(m-n)\omega t}$. After that $\langle n,i|m,j\rangle = \delta_{ij}\delta_{nm}$ can be safely taken because here $|n,i\rangle$s only assign the positions of the components in a vector and their products have nothing to do with the inner product anymore. One can easily verify that the inner product of $|n,i\rangle$ and $|m,j\rangle$ in the new definition is still $\langle n,i|\tilde{W}|m,j\rangle = \delta_{ij}\mathrm{e}^{-\mathrm{i}(m-n)\omega t}$. Although it seems that the number of the set $\{|n,i\rangle\}$ has been increased N times from that of the set $\{|i\rangle\}$, the dimension of the virtual Hilbert space does not increased actually. This is because the metric $\tilde{W}$ is not fully ranked, which can be realized by rewriting the metric as

$$\tilde{W}(t) = \tilde{p}_1(t)\otimes\sum_i|i\rangle\langle i|, \tag{3}$$

where the part of the metric in the virtual direction is

$$\begin{aligned}\tilde{p}_1(t) &= |\tilde{u}_1\rangle\langle\tilde{u}_1|,\\ |\tilde{u}_1\rangle &= \frac{1}{\sqrt{N}}\underbrace{\left(\cdots,\ \mathrm{e}^{-\mathrm{i}(n-1)\omega t},\ \mathrm{e}^{-\mathrm{i}n\omega t}\ \cdots\right)^{\dagger}}_{N}.\end{aligned} \tag{4}$$

So the part of the metric in the virtual direction, $\tilde{p}_1(t)$, has only one rank. This means that only one wavefunction $|\tilde{u}_1\rangle$ is physical and the rest wavefunctions perpendicular to it are inaccessible because their inner products are absolutely zero. This is not strange as no new degree of freedom is actually introduced by Eq. (2).

To make the virtual direction synthetic, the metric on it must be fully ranked. This forces us to introduce a new full rank metric,

$$\tilde{\mathbb{W}} = \sum_{m=1}^{N}\tilde{p}_m(t)\otimes\sum_i|i\rangle\langle i|, \tag{5}$$

where $\tilde{p}_m(t) = |\tilde{u}_m\rangle\langle\tilde{u}_m|$ and

$$|\tilde{u}_m\rangle = \frac{1}{\sqrt{N}}\underbrace{\left(\cdots,\ \mathrm{e}^{-\mathrm{i}(n-1)[\omega t+2\pi(m-1)/N]},\ \mathrm{e}^{-\mathrm{i}n[\omega t+2\pi(m-1)/N]}\ \cdots\right)^{\dagger}}_{N}.$$

The Fourier transformation ensures the orthogonality between the appended metrics, $\tilde{p}_m(t)\tilde{p}_n(t) = \delta_{mn}\tilde{p}_m(t)$, so that they are also the project operators. This is the same as that of the metric I (unit matrix) in ordinary Hilbert space. Although the individual basis $|\tilde{u}_m\rangle(t)$ depends on time explicitly, the total metric $\tilde{\mathbb{W}}$ has a period T/N and becomes a unit matrix when $N\to\infty$. By adopting the artificial metric $\tilde{\mathbb{W}}$, if the effective Hamiltonian matrix, $\tilde{H}$ in Eq. (8), is also independent of time, everything is the same as that in an ordinary Hilbert space. In this sense, we can claim that the dimension is extended by the SD created from Eq. (2) in the time direction. Then the following task is to make these appended $\tilde{p}_m(t)$ physically accessible.

One can easily realize that

$$\tilde{p}_m(t) = \tilde{p}_1[t+2\pi(m-1)/(\omega N)]. \tag{6}$$

So the appended metric $\tilde{p}_m$ at t is equal to a physical metric $\tilde{p}_1$ at $t+2\pi(m-1)/(\omega N)$. By introducing a time shift $t\to t+2\pi(j-1)/(\omega N)$, the total metric $\tilde{\mathbb{W}}$ is invariant because only a rearrangement of $\{\tilde{p}_m\}$ by $m\to m+j\,\mathrm{mod}\,N$ is applied. The details are shown in Table 1. But the evolution of $|\Phi_1\rangle[t+2\pi(j-1)/(\omega N)]$ is

$$\mathrm{i}\partial_t|\Phi_1\rangle\left(\frac{t+2\pi(j-1)}{\omega N}\right) = H\left(\frac{t+2\pi(j-1)}{\omega N}\right)|\Phi_1\rangle\left)\frac{t+2\pi(j-1)}{\omega N}\right).$$

After replacing the physical wavefunction $|\Phi_1\rangle$ at $t+2\pi(j-1)/(\omega N)$ with the virtual wavefunction $|\Phi_j\rangle$ at t, we find the Schrödinger equation for the virtual wavefunctions,

$$\mathrm{i}\partial_t|\Phi_j\rangle(t) = H[t+2\pi(j-1)/(\omega N)]|\Phi_j\rangle(t), \tag{7}$$

which indicates that the evolution of the virtual part of the wavefunction, $\tilde{p}_j|\tilde{\Psi}\rangle(t)$, is guided by a physically accessible Hamiltonian with a shifting time.

Table 1. The metric $\tilde{\mathbb{W}}$ in the synthetic Hilbert space $\{|n,i\rangle\}$ composites both physical metric $\tilde{p}_1(t)$ and virtual metrics $\tilde{p}_m(t)$. The virtual metric $p_m(t)$ at t is equivalent to a physical metric $\tilde{p}_1[t+(m-1)\Delta t]$ at the advanced time $t+(m-1)\Delta t$, where $\Delta t = 2\pi/(N\omega)$. As the Hamiltonian $\tilde{H}$ and metric $\tilde{\mathbb{W}}$ are not dependent on the time explicitly, the effective Hamiltonian for the wavefunction projected by $\tilde{p}_m(t)$, $|\Phi_m\rangle(t) = \tilde{p}_m(t)|\tilde{\Psi}\rangle(t)$, is $H[t+(m-1)\Delta t]$. Here the Hamiltonians, $\tilde{H}$ and $H(t)$, are the matrices appearing in Eqs. (7) and (8), respectively. EPM is short for equivalent physical metric.

	Metric	EPM	Hamiltonian
Physical	$\tilde{p}_1(t)$		$H(t)$
Virtual	$\tilde{p}_2(t)$	$\tilde{p}_1(t+\Delta t)$	$H(t+\Delta t)$
	$\vdots$	$\vdots$	$\vdots$
	$\tilde{p}_m(t)$	$\tilde{p}_1[t+(m-1)\Delta t]$	$H[t+(m-1)\Delta t]$
	$\vdots$	$\vdots$	$\vdots$
	$\tilde{p}_N(t)$	$\tilde{p}_1[t+(N-1)\Delta t]$	$H[t+(N-1)\Delta t]$
Synthetic	$\tilde{\mathbb{W}} = \sum_m \tilde{p}_m(t)$		$\tilde{H}$

After adapting the full rank metric $\tilde{\mathbb{W}}$, the time dependent Hamiltonian $H(t)$ in real space must be mapped to a time independent matrix $\tilde{H}$ whose element is

$$\begin{aligned}\tilde{H}_{ni,mj} &= \langle n,i|\tilde{H}|m,j\rangle \\ &= \frac{1}{T}\int_0^T \langle i|H(t)|j\rangle\, \mathrm{e}^{-\mathrm{i}(m-n)\omega t}\,\mathrm{d}t - \delta_{ij}\delta_{nm}n\omega,\end{aligned}$$

where the last term is caused by a time derivative of $\mathrm{e}^{-\mathrm{i}n\omega t}$ of the basis (gauge factor). Then the evolution of the wavefunction $|\tilde{\Psi}\rangle = \sum_{ni} a_{ni}|n,i\rangle$ in the synthetic Hilbert space becomes

$$\mathrm{i}\frac{\mathrm{d}a_{ni}}{\mathrm{d}t} = \sum_{mj}\tilde{H}_{ni,mj}a_{mj}. \tag{8}$$

3. Wave-packet evolution in synthetic 3D Weyl metal

In this section, we will first consider a diffusion of wave packet in a 3D Weyl metal. The numerical results are presented to illustrate the chiral nature of the Weyl points. From this we confirm that the same results can be obtained based on a 2D model.

The 3D lattice in Fig. 1(a) describes a Weyl metal subjected to electric field E and magnetic field B along the z axis (the electron charge $e=1$),

$$\begin{aligned}H(t) = \sum_{x,y,z}\{&-\mathrm{i}c^\dagger_{x+\delta x,y,z}\sigma_x c_{x,y,z} - \mathrm{i}\,\mathrm{e}^{\mathrm{i}A_y(x)}c^\dagger_{x,y+\delta y,z}\sigma_y c_{x,y,z} \\ &- c^\dagger_{x+\delta x,y,z}\sigma_z c_{x,y,z} - c^\dagger_{x,y+\delta y,z}\sigma_z c_{x,y,z} - c^\dagger_{x,y,z+\delta z}\sigma_z c_{x,y,z} \\ &+ \text{h.c.}\} + Mc^\dagger_{x,y,z}\sigma_z c_{x,y,z} - Ezc^\dagger_{x,y,z}\sigma_0 c_{x,y,z}.\end{aligned} \tag{9}$$

Here $c^\dagger_{x,y,z}$ and $c_{x,y,z}$ are the two components creation and annihilation operators at (x,y,z), $\delta_{x(yz)}$ are the lattice constants along $x(yz)$ and σ's are the Pauli matrices in the two-component space. When $E=0$ and $B=0$, the model will retrieve to the Hamiltonian $H(k_x,k_y,k_z) = 2\sin(k_x)\sigma_x + 2\sin(k_y)\sigma_y + [M - 2\cos(k_x) - 2\cos(k_y) - 2\cos(k_z)]\sigma_z$, where $k_{x(yz)}$ are the momenta along $x(yz)$. It has two Weyl points when $2<|M|<6$, four Weyl points when $|M|<2$ and zero Weyl point when $|M|>6$. Later, we will only discuss the case of $M=-5$ and $B\delta x\delta y = 2\pi/21$. So the magnetic unit cell is 21 times larger than the original unit cell in the xy plane.

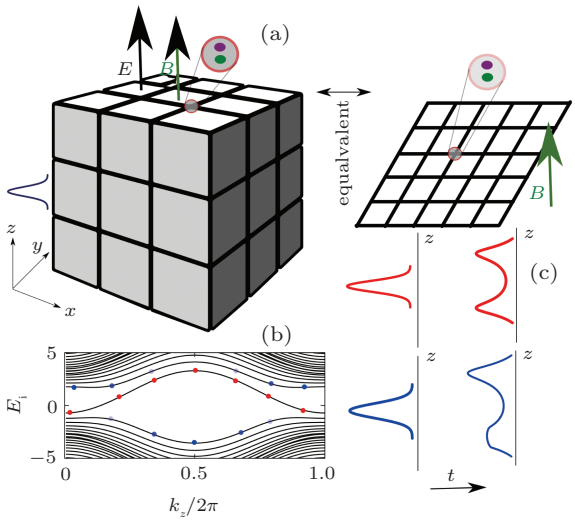


Fig. 1. (color online) (a) Left: The 3D cubic lattice described by Eq. (9). Each site has two internal states standing for spin, orbital or sub-lattice degrees of freedom. External electric field E and magnetic field B are applied in the z direction. Right: The 2D square lattice in Eq. (11). This lattice also has two internal degrees of freedom on each site. A magnetic field B is applied perpendicular to the plane. The Hamiltonians of the two models are the same after extending the SD in time in the 2D model. (b) The spectrum of the 3D lattice when $BS = 2\pi/21$ and $E=0$, where S is the area of one plaquette on the horizontal plane. The dots, whose color depths are standing for the weights $|\langle\phi_i(k_z)|\psi(t=0)\rangle|$, show the initial wave packets $|\psi(t=0)\rangle$ projected on the Landau band eigenstates $|\phi_i(k_z)\rangle$ with red and blue colors distinguishing the two cases. Here i is the index of the Landau levels and the momenta(defined on the magnetic unit cell) on the xy plane are taken as $k_x = k_y = 0$ implicitly for both the wave packets and the eigenstates. (c) In the first case(red), the wave packet will always be symmetric with respect to the $z=0$ plane. But in the second case (blue), the shape of the wave packet should be asymmetric after evolution.

The diffusion of a wave packet is started from the state $\psi(x,y,z,t=0) = \delta(z)\psi^0_{k_x,k_y}(x,y)$, which is a delta function at zero point in the z direction. Its xy components are kept as a plane wave with the good quantum numbers, wave vectors k_x and k_y, defined in the magnetic unit cell. So only the diffusion in the z axis are interested. When $E=0$, k_z restores to be a good quantum number and the dispersion of the Landau levels with respect to k_z is shown in Fig. 1(b). After turning on the electric filed, as long as its strength is much smaller than the spacing between the Landau levels, the tunneling between different Landau levels can be ignored. In this simple Bloch

oscillation scenario, the effect of E is to drag the momentum k_z along each Landau levels with a constant speed. The equation of motion can be summaries as $\dot{z} = \partial E_i/\partial k_z$ and $\dot{k}_z = E$, where the speed of a plane wave in the z direction is equal to its group velocity and E_i is the energy of the ith Landau level.

Because the above equations are for the plane waves in the z direction, correspondingly, we change the representation of the wave packet from the real space to the momentum space. For an initial delta wavefunction, its representation in the momentum space, k_z, is a constant function. But as there are multi Landau levels at each k_z, its components may not smoothly distribute on one Landau level. We schematically show the two case in Fig. 1(b). When the initial wavefunction is equally distributed on one Landau level, indicated by the red points in the figure, its diffusion must be symmetric with respect to the horizontal plane all the time. This can be read from the counteraction of the total group velocity by the wave components with opposite group velocities. In the second case, the initial wave packet is distributed in both the positive and negative Landau levels. In one half of the period, the positive group velocity dominates. While in the other half of period, as long as E has dragged all k_z by one half of the Brillouin zone, the negative group velocity dominates. So the diffusion of the wave packet is asymmetric around $z = 0$. In Fig. 1(c) we plot the typical shapes of the wave packets in both symmetric and asymmetric cases.

In the left column of Fig. 2, we display the diffusions of the wave packets by solving the Schrödinger equation with the 4-th order Rugge–Kutta method. The open boundaries applied in the z direction are far away from the origin so that they will not affect the diffusion. The figures show the weights of the wave packet above and below the $z = 0$ plane with $P_+(t) = \sum_{z>0,x,y} |\psi(x,y,z,t)|^2$ and $P_-(t) = \sum_{z<0,x,y} |\psi(x,y,z,t)|^2$. The wave packet is symmetric with respect to $z = 0$ when $P_+(t) = P_-(t)$, and vice versa. In the right column, we show the projection of the initial states on the eigenstates of distinct Landau bands. Just as we expected, the packets become asymmetric in the second case and keeps symmetric in the first case. But how could a delta wave-function in the z direction can have these two kinds of distributions in the Landau bands? It can be traced back to the chiral nature of the Weyl points. The continuous wave-functions near the Weyl points are the eigenvectors of the Hamiltonian (the group velocity in the z direction and the oscillation frequency have been rescaled to unity)

$$H(k_z) = \begin{pmatrix} \pm k_z & a^\dagger \\ a & \mp k_z \end{pmatrix}, \tag{10}$$

where a and $a^\dagger$ are jumping operators between the Landau levels. A wavefunction $(\phi_0(x,y),0)^{\mathrm{T}}\delta(z)$ is weighted equally in the 0-th Landau bands $(\phi_0(x,y),0)^{\mathrm{T}}\mathrm{e}^{\mathrm{i}k_z z}$. Here $\phi_0(x,y)$ is the 0-th Landau wavefunction in the xy plane. But for the n-th Landau bands with the energy $+\sqrt{k_z^2+n}$, the eigenstate changes to $(\alpha\phi_n(x,y), \beta\phi_{n-1}(x,y))^{\mathrm{T}}\mathrm{e}^{\mathrm{i}k_z z}$, where $|\alpha/\beta| = \sqrt{n}/|k_z - \sqrt{k_z^2+n}|$. We notice that this ratio is changed from less than 0.5 to larger than 0.5 when k_z is passing the Weyl point at $k_z = 0$. So if the delta packet we prepared is strongly weighted on this band when $k_z < 0$, such weight should decrease when $k_z > 0$. In compensation, the amplitude of the projection on the negative energy bands should be increased. This forms the second layout of the projection shown in Fig. 1(b).

The last interesting property of the diffusion is that the unbalanced diffusion can be observed on a randomly initial wave-packet. As shown in Fig. 2, the packet is still delta in the z direction, but is randomly prepared in the magnetic unit cell in the x–y plane. Our numerical calculation indicates that its diffusion is still unbalanced. The reason behind this phenomenon is that such kind of random packet still has a bias distribution in the Landau bands, shown in the right corner of Fig. 2.

Now we come back to a 2D lattice reading as

$$\begin{aligned} H(t) = \sum_{x,y} \{ & -\mathrm{i}c^\dagger_{x+\delta x,y}\sigma_x c_{x,y} - \mathrm{i}\,\mathrm{e}^{\mathrm{i}A_y(x)}c^\dagger_{x,y+\delta y}\sigma_y c_{x,y} \\ & + [M - 2\cos(\omega t)]c^\dagger_{x,y}\sigma_z c_{x,y} \\ & - c^\dagger_{x+\delta x,y}\sigma_z c_{x,y} - c^\dagger_{x,y+\delta y}\sigma_z c_{x,y} + \mathrm{h.c.}\}. \end{aligned} \tag{11}$$

In the framework spanned by $\{|n,x,y\rangle = \mathrm{e}^{-\mathrm{i}n\omega t}|x,y\rangle\}$, the Hamiltonian becomes

$$\begin{aligned} \tilde{H} = \sum_{n,x,y} \{ & -\mathrm{i}c^\dagger_{n,x+\delta x,y}\sigma_x c_{n,x,y} - \mathrm{i}\,\mathrm{e}^{\mathrm{i}A_y(x)}c^\dagger_{n,x,y+\delta y}\sigma_y c_{n,x,y} - c^\dagger_{n,x+\delta,y}\sigma_z c_{n,x,y} - c^\dagger_{n,x,y+\delta y}\sigma_z c_{n,x,y} - c^\dagger_{n+1,x,y}\sigma_z c_{n,x,y} + \mathrm{h.c.}\} \\ & + M c^\dagger_{n,x,y}\sigma_z c_{n,x,y} - \omega n c^\dagger_{n,x,y}\sigma_0 c_{n,x,y}, \end{aligned}$$

where $c_{n,x,y}$ ($c^\dagger_{n,x,y}$) are the second quantization operators of the Dirac brackets $\langle n,x,y|$ ($|n,x,y\rangle$). For a wavefunction $|\tilde{\Psi}\rangle = \sum_{n,x,y} a_{n,x,y}|n,x,y\rangle$, its evolution is restricted by the Schrödinger equation $\mathrm{i}\,\mathrm{d}\boldsymbol{a}/\mathrm{d}t = \tilde{H}\boldsymbol{a}$. So the evolution of $\{a_{n,x,y}\}$ is identical to the components of a wavefunction in the above Weyl lattice when $\omega = E$.

But in representing $|\tilde{\Psi}\rangle(t)$, we must remember that the inner product has been redefined by the metric $\tilde{\mathbb{W}}$. Among this artificial metric, the physical part is $\tilde{p}_1(t)$ and the corresponding physical wavefunction is

$$|\Phi_1\rangle(t) = \tilde{p}_1(t)|\tilde{\Psi}\rangle(t) = \sum_{x,y}\left(\frac{1}{\sqrt{N}}\sum_n a_{n,x,y}(t)\,\mathrm{e}^{-\mathrm{i}n\omega t}\right)|x,y\rangle.$$

Its evolution, by substituting $\dot{a}_{n,x,y}$ into it, is $\mathrm{i}\partial_t|\Phi_1\rangle(t) = H(t)|\Phi_1\rangle(t)$. One will realize that the Schrödinger equation for the physical wavefunction in 2D system is restored. While for the appended part of the metric $\tilde{p}_m(t)$ with $m > 1$, their corresponding virtual wavefunctions are

$$|\Phi_m\rangle(t) = \tilde{p}_m(t)|\tilde{\Psi}\rangle(t) = \sum_{x,y}\left(\frac{1}{\sqrt{N}}\sum_n a_{n,x,y}(t)\,\mathrm{e}^{-\mathrm{i}n(\omega t+2\pi(m-1)/N)}\right)$$

and their evolution, after substituting $\dot{a}_{n,x,y}$, are $\mathrm{i}\partial_t|\Phi_m\rangle(t) = H(t+2\pi(m-1)/(\omega N))|\Phi_m\rangle(t)$. This means that the evolution of the virtual wavefunctions are still accessible in the 2D system by a shift of time in the Hamiltonian.

Because the z direction in the 3D model is synthesized by the n and the Fourier transformation of a delta function is a constant function, we prepare a series of 2D lattices with identical initial wave-packets. The elements of this ensemble is indexed by $j = 1,\ldots,N$. On the j-th lattice, we start the evolution at $t = 0$ with the Hamiltonian $H(t+2\pi(j-1)/N)$. The evolution of each wave packet in the ensemble are calculated by the 4-th order Rugge–Kutta method. To restore the representation in the n (z) direction, An inverse Fourier transformation is employed in the ensemble. So the wavefunction at n (z) in time t is $\psi_n(x,y)(t) = (1/\sqrt{N})\sum_j \mathrm{e}^{\mathrm{i}nj}\psi_j(x,y)(t)$. We also plot the weights $P_-(t)$ and $P_+(t)$ for $n < 0$ and $n > 0$ for several kinds of initial wave-packets. These results are identical to those in Fig. 2.

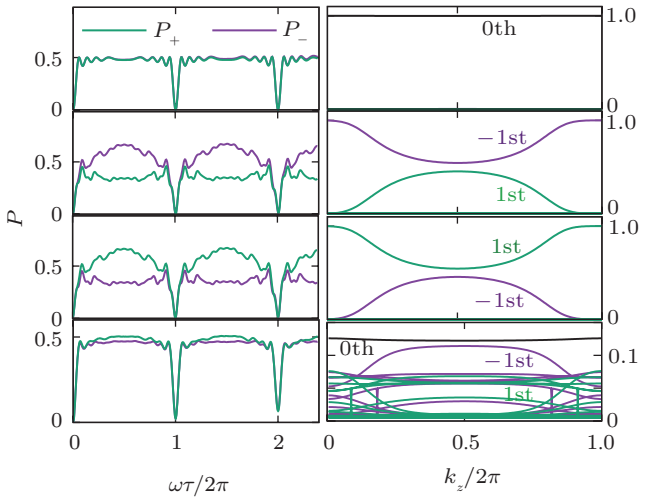


Fig. 2. (color online) Left column: The weights of the wave packet P_+ and P_- versus time t. Rigth column: The projection of the initial wave packet on the Landau bands. Here we show the diffusion in the z direction for 4 kinds of initial packets $\psi^0_{k_x=0,k_y=0}(x,y)$ on the xy plane. The last row is for a random pre-normalized initial packet, $\psi^0(x,y) = a+ib$, with a and b are randomly chosen in $[-0.5,0.5]$. The results shown here are averaged over 1000 random configurations. The projections to the 0-th and $\pm$1st Landau levels are indicated in the right corner, while the projections on the other Landau levels are shown but not indicated explicitly.

4. Conclusions and discussions

We understand the framework of extended Hilbert space with the help of the metric in this space. Although the dimension of time is only one, it can produce as many SDs as needed. For instance, when the Hamiltonian is $H(t) = H_0 + H_1(\omega_1 t) + H_2(\omega_2 t)$ with incommensurate ω_1 and ω_2, 2 SDs can be generated by $|n,m,i,j\rangle = \mathrm{e}^{-\mathrm{i}n\omega_1 t}\mathrm{e}^{-\mathrm{i}m\omega_2 t}|i,j\rangle$, which is similar to that in the Floquet framework.[32] So by subjecting a 2D system into the time-varying potential with two incommensurate frequencies, one will able to simulate a four-dimensional model. This may be used to studies the transport in the models with nonzero second kind of Chern numbers.

When considering the modulate time as a parameter, this approach is, in principle, similar to the other proposals based on parameters. But as the SD here is along the direction of energy, the framework is flexible when a boundary or a domain wall is needed in the SD. They may be realized when a damping mechanics is enrolled. Typically the damping caused by phonons in the environment has a threshold in the energy. It is not active when the energy is smaller than the minimal energy of the phonons Ω_c. So the SD can be effectively separated into two domains by the condition $|n\omega| \sim \Omega_c$. These two regions will have different effective temperatures depending on whether the damping is acted or not. This topic can be investigated to study the topological protected boundary state in the SD.

We also show that the Bloch oscillation in 3D Weyl metal can be simulated exactly on a 2D insulator subjected to both periodic on-site potential and perpendicular magnetic field. The diffusion can be asymmetric when the initial wave packet is not on the 0th Landau level. This is different from the chiral anomaly, which relies on the unbalanced electrons on the 0th Landau level.

References

[1] Wu Z, Zhang L, Sun W, *et al.* 2016 *Science* **354** 83
[2] Eriksson E, Riwar R P, Houzet M, Meyer J S and Nazarov Y V 2017 *Phys. Rev. B* **95** 075417
[3] Meyer J S and Houzet M 2017 *Phys. Rev. Lett.* **119** 136807
[4] Ozawa T and Carusotto I 2017 *Phys. Rev. Lett.* **118** 013601
[5] Ozawa T, Price H M, Goldman N, Zilberberg O and Carusotto I 2016 *Phys. Rev. A* **93** 043827
[6] Riwar R P, Houzet M, Meyer J S and Nazarov Y V 2016 *Nat. Commun.* **7** 11167
[7] Schroer M, Kolodrubetz M, Kindel W, *et al.* 2014 *Phys. Rev. Lett.* **113** 050402
[8] Wang Q, Xiao M, Liu H, Zhu S and Chan C 2017 *Phys. Rev. X* **7** 031032
[9] Yu J, Xu Z F, Lu R and You L 2016 *Phys. Rev. Lett.* **116** 143003
[10] Zhang D W and Yang X C 2016 *Quantum Information Processing* **15** 1909
[11] Harper P G 1955 *Proc. Phys. Soc. London Sect. A* **68** 874
[12] Lau A and Ortix C 2015 *Phys. Rev. Lett.* **115** 216805
[13] Aubry S and Andr G 1980 *Ann. Isr. Phys. Soc.* **3** 133
[14] Price H M, Zilberberg O, Ozawa T, Carusotto I and Goldman N 2015 *Phys. Rev. Lett.* **115** 195303
[15] Price H M, Zilberberg O, Ozawa T, Carusotto I and Goldman N 2016 *Phys. Rev. B* **93** 245113
[16] Else D V, Bauer B and Nayak C 2016 *Phys. Rev. Lett.* **117** 090402
[17] Erker P, Mitchison M T, Silva R, *et al.* 2017 *Phys. Rev. X* **7** 031022
[18] Li T, Gong Z X, Yin Z Q, *et al.* 2012 *Phys. Rev. Lett.* **109** 163001

[19] Shapere A and Wilczek F 2012 *Phys. Rev. Lett.* **109** 160402
[20] Watanabe H and Oshikawa M 2015 *Phys. Rev. Lett.* **114** 251603
[21] Budich J C, Hu Y and Zoller P 2017 *Phys. Rev. Lett.* **118** 105302
[22] Dehghani H and Mitra A 2016 *Phys. Rev. B* **93** 205437
[23] Else D, Bauer B and Nayak C 2017 *Phys. Rev. X* **7** 011026
[24] Floquet G 1883 *On Linear Differential Equation with Periodic Coefficients* (Annales Scientifiques de l'cole Normale Suprieure)
[25] Harper F and Roy R 2017 *Phys. Rev. Lett.* **118** 115301
[26] Khemani V, Lazarides A, Moessner R and Sondhi S L 2016 *Phys. Rev. Lett.* **116** 250401
[27] Kibis O V, Dini K, Iorsh I V and Shelykh I A 2017 *Phys. Rev. B* **95** 125401
[28] Kolodrubetz M, Fregoso B M and Moore J E 2016 *Phys. Rev. B* **94** 195124
[29] Lellouch S, Bukov M, Demler E and Goldman N 2017 *Phys. Rev. X* **7** 021015
[30] Leykam D, Rechtsman M C and Chong Y D 2016 *Phys. Rev. Lett.* **117** 013902
[31] Lindner N H, Berg E and Rudner M S 2017 *Phys. Rev. X* **7** 011018
[32] Martin I, Refael G and Halperin B 2017 *Phys. Rev. X* **7** 041008
[33] Mori T, Kuwahara T and Saito K 2016 *Phys. Rev. Lett.* **116** 120401
[34] Morimoto T, Po H C and Vishwanath A 2017 *Phys. Rev. B* **95** 195155
[35] Nandy S, Sen A and Sen D 2017 *Phys. Rev. X* **7** 031034
[36] Po H C, Fidkowski L, Morimoto T, Potter A C and Vishwanath A 2016 *Phys. Rev. X* **6** 041070
[37] Potirniche I D, Potter A C, Schleier M, Vishwanath A and Yao N Y 2017 *Phys. Rev. Lett.* **119** 123601
[38] Potter A C and Morimoto T 2017 *Phys. Rev. B* **95** 155126
[39] Restrepo S, Cerrillo J, Bastidas V M, Angelakis D G and Brandes T 2016 *Phys. Rev. Lett.* **117** 250401
[40] Roy R and Harper F 2016 *Phys. Rev. B* **94** 125105
[41] Roy R and Harper F 2017 *Phys. Rev. B* **95** 195128
[42] Roy R and Harper F 2017 *Phys. Rev. B* **96** 155118
[43] Von Keyserlingk C W and Sondhi S L 2016 *Phys. Rev. B* **93** 245145
[44] Novičenko V, Anisimovas E and Juzeliūnas G 2017 *Phys. Rev. A* **95** 023615
[45] Sambe H 1973 *Phys. Rev. A* **7** 2203